Electronic Journal of Biotechnology 82 (2026) 100717

Contents lists available at ScienceDirect

Electronic Journal of Biotechnology

journal homepage: www.elsevier.com/locate/ejbt

Research article

ABL1-STAT3-NLRP3 axis attenuates pyroptosis and alleviates diabetic retinopathy ☆

Lili Hu [a], Gong Chen [b], Haoning Pan [c], Shaoxin Pan [a,*]

[a] Ophthalmology Medical Center, The Second Affiliated Hospital of Wannan Medical College, Wuhu, Anhui Province, the People's Republic of China
[b] Cancer Medical Center, Renmin Hospital of Wuhan University, Wuhan, Hubei Province, the People's Republic of China
[c] Wannan Medical College, Wuhu, Anhui Province, the People's Republic of China

GRAPHICAL ABSTRACT

ABL1-STAT3-NLRP3 axis attenuates pyroptosis and alleviates diabetic retinopathy

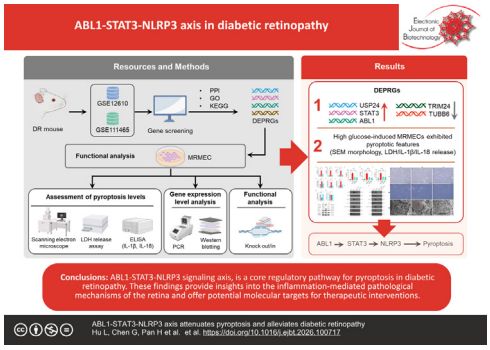

ARTICLE INFO

Article history:
Received 26 December 2025
Accepted 19 May 2026
Available online 12 June 2026

Keywords:
ABL1
Biomarkers
Diabetic retinopathy
High-glucose exposure
Inflammation
Interleukin-18
Interleukin-1β
NLRP3 inflammasome

ABSTRACT

Background: Diabetic retinopathy is a major microvascular complication of diabetes and a leading cause of vision loss. Persistent low-grade inflammation drives disease progression. Pyroptosis, characterized by its pro-inflammatory nature, is involved in several inflammatory diseases, yet the molecular mechanisms specific to diabetic retinopathy remain largely undefined. This study aimed to identify the key molecular drivers and regulatory pathways of pyroptosis in diabetic retinopathy.
Results: Five key pyroptosis-related genes were identified: ubiquitin-specific peptidase 24, signal transducer and activator of transcription 3, and ABL proto-oncogene 1 were upregulated, while tripartite motif containing 24 and tubulin beta 6 class VI were downregulated in diabetic retinopathy. High glucose exposure induced pyroptotic morphology and increased lactate dehydrogenase, interleukin-1 beta, and interleukin-18 levels. Functional assays demonstrated that ABL proto-oncogene 1 acts upstream of signal transducer and activator of transcription 3 to activate the NOD-like receptor family pyrin domain-containing 3 inflammasome, ultimately leading to pyroptosis. Signal transducer and activator of transcription 3 showed strong diagnostic value with an area under the curve exceeding 0.9.

Abbreviations: DR, Diabetic retinopathy; PRGs, pyroptosis-related genes; DEGs, differentially expressed genes; DEPRGs, differentially expressed pyroptosis-related genes; PPI, protein-protein interaction; GEO, Gene Expression Omnibus; GO, Gene Ontology; BP, biological processes; MF, molecular functions; CC, cellular components; KEGG, Kyoto Encyclopedia of Genes and Genomes; RBPs, RNA-binding proteins; TFs, transcription factors; ROC, receiver operating characteristic; AUC, area under the curve; Tfh, T follicular helper; MRMEC, mouse retinal microvascular endothelial cell; SEM, scanning electron microscopy; LDH, lactate dehydrogenase; NK cells, natural killer cells.

☆ Audio abstract available in Supplementary material.

Peer review under responsibility of Pontificia Universidad Católica de Valparaíso.

* Corresponding author.
E-mail address: 20222058@wnmc.edu.cn (S. Pan).

https://doi.org/10.1016/j.ejbt.2026.100717

Programmed cell death
Pyroptosis
STAT3

Conclusions: This study identifies a novel ABL proto-oncogene 1–signal transducer and activator of transcription 3–NOD-like receptor family pyrin domain containing 3 signaling axis as a central regulator of pyroptosis in diabetic retinopathy. These findings provide insights into inflammation-induced retinal pathology and suggest candidate molecular targets for therapeutic intervention.

How to cite: Hu L, Chen G, Pan H, et al. ABL1-STAT3-NLRP3 axis attenuates pyroptosis and alleviates diabetic retinopathy. Electron J Biotechnol 2026;82. https://doi.org/10.1016/j.ejbt.2026.100717.

1. Introduction

Diabetic retinopathy (DR) arises as a chronic microvascular consequence of diabetes mellitus and continues to be a primary global cause of preventable blindness and vision deterioration in middle-aged adults [1]. The disease involves progressive damage to the retinal microvasculature, presenting clinically with microaneurysms, hemorrhages, lipid exudates, macular edema, capillary nonperfusion, and, in advanced stages, fibrovascular proliferation and retinal detachment [2]. The escalating global prevalence of diabetes is expected to drive a parallel surge in DR cases, representing a significant public health challenge with socioeconomic consequences [3]. Current therapeutic strategies for DR, such as intravitreal administration of anti–vascular endothelial growth factor (anti-VEGF) agents and vitreoretinal surgery, have demonstrated effectiveness in suppressing neovascularization and managing macular edema [4]. However, these treatments are limited by high cost, invasive procedures, frequent recurrence, and variable responses across patient populations. Moreover, existing therapies mainly focus on vascular pathology and fail to modulate the underlying inflammatory and neurodegenerative processes. Importantly, they fail to reverse established damage to the neural retina, underscoring that the molecular mechanisms underlying DR pathogenesis must be explored to develop more effective and sustainable therapeutic approaches [5]. Persistent low-grade inflammation is a key cause of retinal injury in DR. Among the inflammatory mechanisms implicated in retinal degeneration, pyroptosis has attracted increasing attention [6]. Pyroptosis represents a destructive, inflammation-driven mode of programmed cell death that mechanistically diverges from both apoptosis and necroptosis [7]. It is triggered by inflammasome activation, which induces cleavage of gasdermin D (GSDMD) and the formation of transmembrane pores, resulting in osmotic cell swelling, membrane rupture, and the massive release of proinflammatory cytokines, notably interleukin-1β (IL-1β) and interleukin-18 (IL-18) [8]. The consequent cytokine surge amplifies local inflammation, compromises the blood–retinal barrier, and promotes vascular and neuronal injury within the retina [9]. Emerging evidence implicates pyroptosis in multiple ocular disorders, such as age-related macular degeneration, glaucoma, and autoimmune uveitis, indicating its broader contribution to retinal pathogenesis [10]. Although early evidence links pyroptosis to DR, the specific upstream regulators and signaling cascades responsible for its activation in the diabetic retina have yet to be comprehensively investigated [11]. To bridge this knowledge gap, an integrated approach was employed that combined bioinformatic analysis of retinal transcriptomic datasets (GSE12610 and GSE111465) with *in vitro* experimental validation. By intersecting differentially expressed genes (DEGs) from DR models with a curated database of pyroptosis-related genes, we identified five core candidates. Among these, ubiquitin-specific peptidase 24 (USP24), signal transducer and activator of transcription 3 (STAT3), and ABL proto-oncogene 1 (ABL1) exhibited significant upregulation, whereas tripartite motif containing 24 (TRIM24) and tubulin beta 6 class VI (TUBB6) exhibited marked downregulation in diabetic retinal tissue. These findings were corroborated in a high-glucose-induced model of mouse retinal microvascular endothelial cells (MRMECs), which displayed classic pyroptotic morphology and elevated release of lactate dehydrogenase (LDH), IL-1β, and IL-18. Further mechanistic analyses revealed that silencing either STAT3 or ABL1 significantly attenuated pyroptotic markers. In rescue experiments, overexpression of ABL1 enhanced pyroptosis, whereas concurrent knockdown of STAT3 markedly suppressed this effect, supporting a hierarchical regulatory model in which ABL1 operates upstream of STAT3 to promote NOD-like receptor family pyrin domain containing 3 (NLRP3) inflammasome activation and drive pyroptotic cell death.

Collectively, our findings define a novel molecular module involved in pyroptosis and propose an ABL1–STAT3–NLRP3 signaling axis as a key contributor to inflammatory damage in DR. This work enhances the understanding of pyroptosis in the diabetic retina and identifies promising molecular targets for precision therapies aimed at halting or reversing inflammation-mediated retinal injury.

2. Materials and methods

2.1. Data source

Two retinal transcriptomic datasets, GSE12610 (GPL12610 platform; 3 DR vs. 2 control mouse retinas) and GSE111465 (GPL1355 platform; 6 DR vs. 6 controls), were downloaded from the Gene Expression Omnibus (GEO) database. The raw data were subjected to background correction, normalization, and standardization using the limma package in R to eliminate batch-dependent variation. To construct a comprehensive reference panel of pyroptosis-related genes (PRGs), genes annotated in GeneCards, Gene Set Enrichment Analysis (GSEA), and PubMed under the search terms "pyroptosis" and "pyroptosis-associated genes" were compiled into a unified dataset for downstream analysis. After removal of duplicates, 322 unique PRGs were retained for downstream analysis.

2.2. Identification of pyroptosis-related differentially expressed genes

Differential gene expression analysis between DR and control samples was conducted using the DESeq2 package in R. Genes exhibiting a $|\log_2 \text{fold change}| > 0$ with a p value < 0.05 were classified as differentially expressed. The resulting transcriptional profiles were illustrated using volcano plots and heatmaps produced using the ggplot2 and pheatmap packages to highlight global expression trends and group-specific clustering. Overlapping DEGs between datasets were intersected with the curated PRG set to obtain pyroptosis-related differentially expressed genes (DEPRGs). Venn diagrams were plotted to illustrate the intersecting gene sets.

2.3. Protein-protein interaction (PPI) network and hub gene analysis

PPI mapping of the identified DEPRGs was carried out using the STRING database (v11), applying a confidence cutoff of 0.4 to exclude weak associations. The curated interaction network was then reconstructed and examined in Cytoscape, enabling visualization of molecular connectivity patterns and identification of central hub proteins within the network. To identify central regulatory genes, five algorithms within the cytoHubba plugin, namely, degree, MNC, MCC, closeness, and EPC, were applied. Genes consistently ranked among the top candidates by all five algorithms were considered hub genes and were used for subsequent analyses.

2.4. Functional enrichment analysis

The biological relevance of DEPRGs was examined through enrichment analyses implemented in the clusterProfiler package in R. Gene Ontology (GO) annotation was used to classify genes according to their involvement in biological processes (BPs), molecular functions (MFs), and cellular components (CCs). Functional pathway enrichment was performed using the Kyoto Encyclopedia of Genes and Genomes (KEGG) database to uncover signaling pathways linked to the identified genes. Pathways with both p values and false discovery rates (FDRs) of <0.05 were considered statistically significant, with multiple comparisons adjusted using Benjamini–Hochberg correction to control for false positives. GO semantic similarity between DEPRGs was calculated using the 'GOSemSim' package to evaluate functional relationships.

2.5. ceRNA network construction

To investigate posttranscriptional regulatory mechanisms, interactions between miRNAs and DEPRGs were retrieved from miRTarBase and StarBase. Candidate long noncoding RNAs (lncRNAs) and circular RNAs (circRNAs) that could bind to these miRNAs were obtained from LncBase and StarBase. The resulting lncRNA–miRNA–mRNA and circRNA–miRNA–mRNA interaction networks were then assembled and visualized in Cytoscape, providing insight into the ceRNA-mediated regulation of pyroptosis.

2.6. RBP/TF/Drug regulatory networks

RNA-binding proteins (RBPs) potentially interacting with DEPRGs were predicted using StarBase, while transcription factors (TFs) regulating DEPRGs were identified through ChIPBase and hTFtarget. Information on potential drug–gene interactions was retrieved from the Comparative Toxicogenomics Database. Integrated visualization of RBP, TF, and drug interaction networks was performed in Cytoscape to elucidate potential regulatory and pharmacological relationships.

2.7. Immune infiltration analysis

To characterize DR-related immune microenvironment changes, CIBERSORTx analysis was performed using the LM22 leukocyte signature matrix to estimate immune cell proportions. Samples with $p < 0.05$ were retained to ensure analytical reliability. Correlation analysis between DEPRGs and immune cell abundance was conducted using Spearman's rank correlation, revealing key links between pyroptotic activity and immune regulation within the retinal microenvironment.

2.8. Validation and diagnostic efficacy

Expression differences of DEPRGs between DR and control samples were validated in both transcriptomic datasets. The diagnostic potential of each gene was assessed by constructing receiver operating characteristic (ROC) curves using the pROC package in R, with the area under the curve (AUC) serving as a quantitative measure of classification performance, with values of 0.5–0.7 indicating limited discrimination, 0.7–0.9 indicating moderate discrimination, and values >0.9 indicating strong diagnostic potential.

2.9. Cell culture and hyperglycemic model

Mouse retinal microvascular endothelial cells (MRMECs) were sourced from Procell (China) and maintained in endothelial cell growth medium under standard culture conditions. To simulate the hyperglycemic environment characteristic of DR, cells were exposed to 30 mM D-glucose (MCE, HY-B0389) for 48 h to induce hyperglycemic stress. Two control conditions were used: a normal-glucose group cultured in 5 mM D-glucose and an osmotic control consisting of 5 mM D-glucose plus 25 mM D-mannitol (MCE, HY-N0378) to account for osmotic pressure effects.

2.10. Assessment of pyroptosis

Cells were first immobilized in 2.5% glutaraldehyde, followed by stepwise dehydration in graded ethanol concentrations. After critical-point drying, the cellular ultrastructure was examined through scanning electron microscopy (SEM; Hitachi SU8010; accelerating voltage = 5 kV). Characteristic morphological features, such as cell swelling and membrane pore formation, were documented. Pyroptotic activity was evaluated by quantifying LDH released into the culture medium using the CytoTox 96® Non-Radioactive Cytotoxicity Assay (Servicebio). Secreted IL-1β and IL-18 levels were determined using ELISA kits (Absin; IL-1β: 510002-96T, IL-18: 510003-96T). Absorbance readings were obtained at 490 nm, and LDH release was normalized to total cellular LDH content to estimate the proportion of cells undergoing membrane rupture, serving as a quantitative marker of pyroptotic cell death.

2.11. Gene expression analysis

2.11.1. Quantitative real-time PCR (qRT-PCR)

Total RNA extraction was carried out with TRIzol reagent (Servicebio, G3013), followed by reverse transcription of 1 μg RNA into complementary DNA using PrimeScript RT Master Mix (Servicebio, G3323). Gene expression quantification was performed via SYBR Green–based real-time PCR on a Roche LightCycler 96 platform. Expression of the target genes, namely, USP24, TUBB6, TRIM24, STAT3, and ABL1, was normalized to GAPDH, and relative transcript abundance was determined using the 2^−ΔΔCt method.

2.11.2. Western blot analysis

Total protein was extracted using RIPA lysis buffer supplemented with protease and phosphatase inhibitors to prevent enzymatic degradation. Protein concentration was quantified using the BCA assay, and 20–30 μg of each sample was loaded onto 10% SDS–polyacrylamide gels for electrophoretic separation, followed by transfer to PVDF membranes. Membranes were blocked with 5% nonfat milk for 1 hour and incubated overnight at 4 °C with primary antibodies against STAT3, ABL1, USP24, TRIM24, TUBB6, NLRP3, Caspase-1, Cleaved Caspase-1, GSDMD, GSDMD-N, ASC, and GAPDH (loading control).. After washing, the membranes were incubated with HRP-conjugated secondary antibodies, and signal detection was performed using enhanced chemiluminescence reagents.

2.12. Gene knockdown and overexpression

Small interfering RNAs (siRNAs) targeting mouse STAT3 and ABL1, along with a nontargeting control, were synthesized by GenePharma (China). For overexpression assays, the full-length ABL-1 cDNA was inserted into the pcDNA3.1 vector. Mouse retinal microvascular endothelial cells (MRMECs) were transfected with 50 nM siRNA or 2 μg plasmid DNA using Lipofectamine 3000 (Invitrogen). Transfection outcomes were assessed 24 h post-transfection by qRT-PCR and Western blot to confirm gene silencing or overexpression efficiency. Cells were exposed to high glucose (25 mM) for 48 h to establish an *in vitro* diabetic retinopathy model. Pyroptosis was evaluated by measuring LDH release, secreted levels of IL-1β and IL-18 (by ELISA), and pyroptotic markers protein expression of NLRP3, caspase-1, cleaved caspase-1, GSDMD, GSDMD-N, and ASC (by Western blotting). To dissect the ABL1-STAT3 hierarchy, rescue experiments were performed by first transfecting with ABL1 overexpression plasmid, followed by STAT3-targeting siRNA (48 h later). Cells were then cultured under high glucose and pyroptotic markers were measured.

2.13. Statistical analysis

Data are expressed as the mean ± SD from a minimum of three independent biological replicates. For comparisons between two groups, statistical significance was assessed using either Student's *t* test for normally distributed data or the Mann–Whitney *U* test for nonparametric data. For experiments involving multiple groups, one-way ANOVA followed by Tukey's multiple comparison test was applied to identify significant pairwise differences. A p value < 0.05 was considered indicative of statistical significance.

3. Results

3.1. Data quality control and DEPRG identification

Principal component analysis revealed distinct clustering of DR and control retinal samples in both the GSE12610 and GSE111465 datasets, indicating clear transcriptomic divergence and validating the datasets for subsequent differential expression analysis. The overall study design is illustrated in Fig. 1. In the GSE12610 dataset, transcriptomic profiling revealed 39,860 DEGs, with 18,750 genes showing increased and 21,110 showing decreased expression levels (Fig. 2A,C). Similarly, analysis of the GSE111465 dataset identified 24,857 DEGs, including 11,993 upregulated and 12,864 downregulated transcripts (Fig. 2B,D). Integrative comparison of both DEG datasets with a curated pyroptosis-related gene panel uncovered five overlapping genes, which were designated DEPRGs representing the key molecular link between diabetic retinopathy and pyroptotic signaling: USP24, STAT3, and ABL1 were consistently upregulated, whereas TRIM24 and TUBB6 were downregulated (Fig. 2E and Table 1). Correlations among these five DEPRGs are visualized in Fig. 2F.

3.2. Functional enrichment analysis

Functional similarity analysis indicated that TRIM24, STAT3, and ABL1 play central roles in DR pathogenesis (Fig. 3A,B). PPI analysis revealed 13 interacting partners (Fig. 3C). Enrichment analysis indicated the participation of the identified genes in phosphorylation-dependent regulatory mechanisms, particularly protein autophosphorylation and peptidyl-tyrosine modification (GO-BP; Fig. 3D and Table 2). Cellular component analysis (GO-

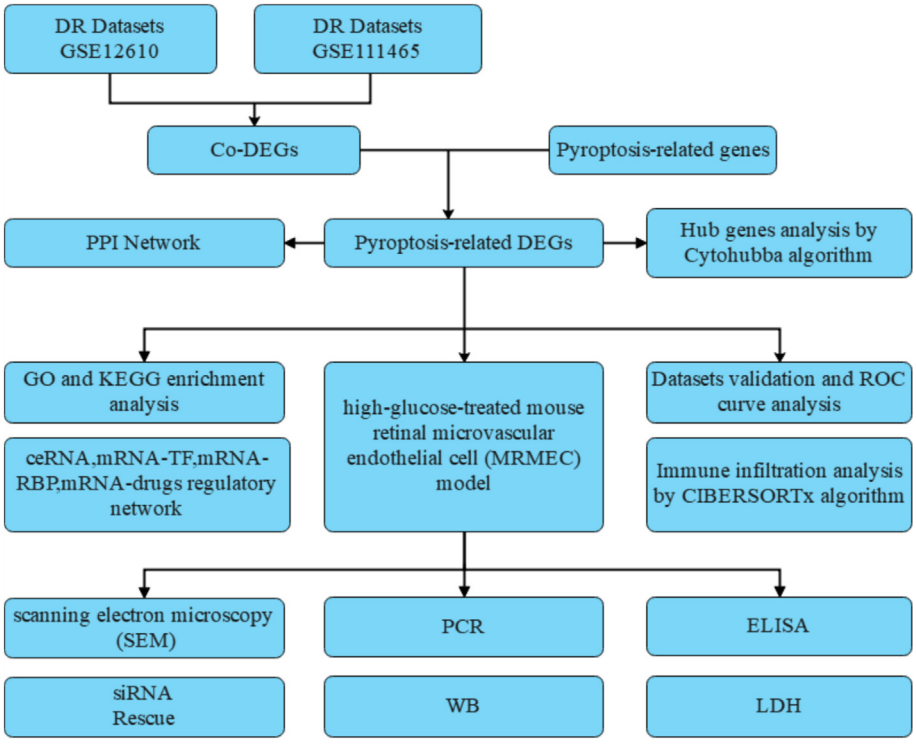

Fig. 1. Flow chart for the comprehensive analysis of pyroptosis-related DEGs.

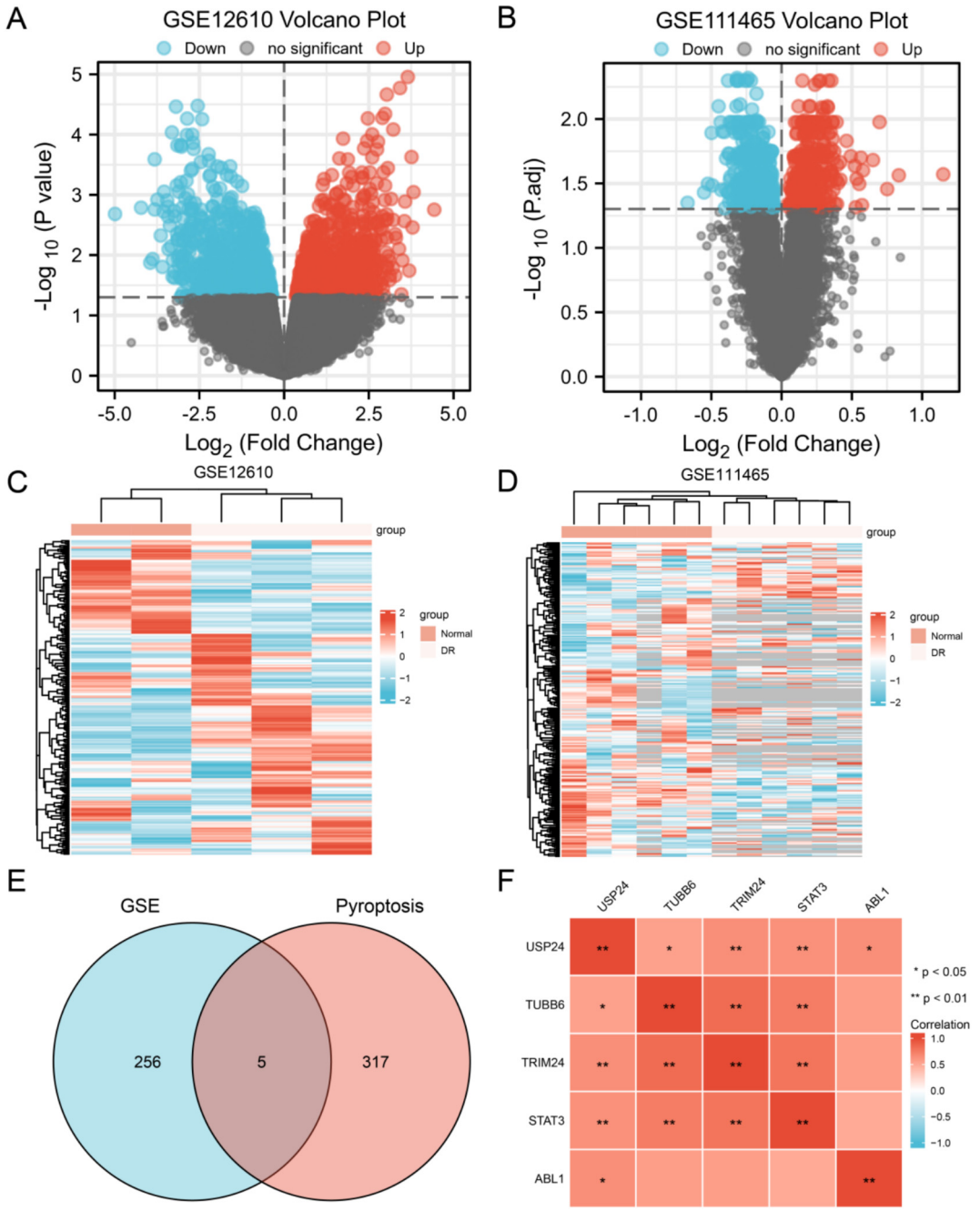

Fig. 2. Diabetic retinopathy differential gene expression analysis. A-B. Volcano map of the differentially expressed genes in the GSE12610 dataset (A) and GSE111465 dataset (B). C-D. Co-DEG heatmap in the GSE12610 dataset (C) and GSE111465 dataset (D). Venn diagram of pyroptosis-related genes plotted against the Co-DEGs (E). Correlation heatmap of DEPRGs (F). DR, diabetic retinopathy; Co-DEGs, common differentially expressed genes; DEPRGs, differentially expressed pyroptosis-related genes.

Table 1
Pyroptosis-related regulated DEGs.

Gene symbol	Description	GC Id	Relevance score
USP24	Ubiquitin Specific Peptidase 24	GC01M055066	0.153248027
TUBB6	Tubulin Beta 6 Class V	GC18P012307	0.433450878
TRIM24	Tripartite Motif Containing 24	GC07P138460	1.256297112
STAT3	Signal Transducer and Activator of Transcription 3	GC17M042313	2.512526512
ABL1	ABL Proto-Oncogene 1, Non-Receptor Tyrosine Kinase	GC09P130713	1.207589269

DEGs: Differentially Expressed Genes.

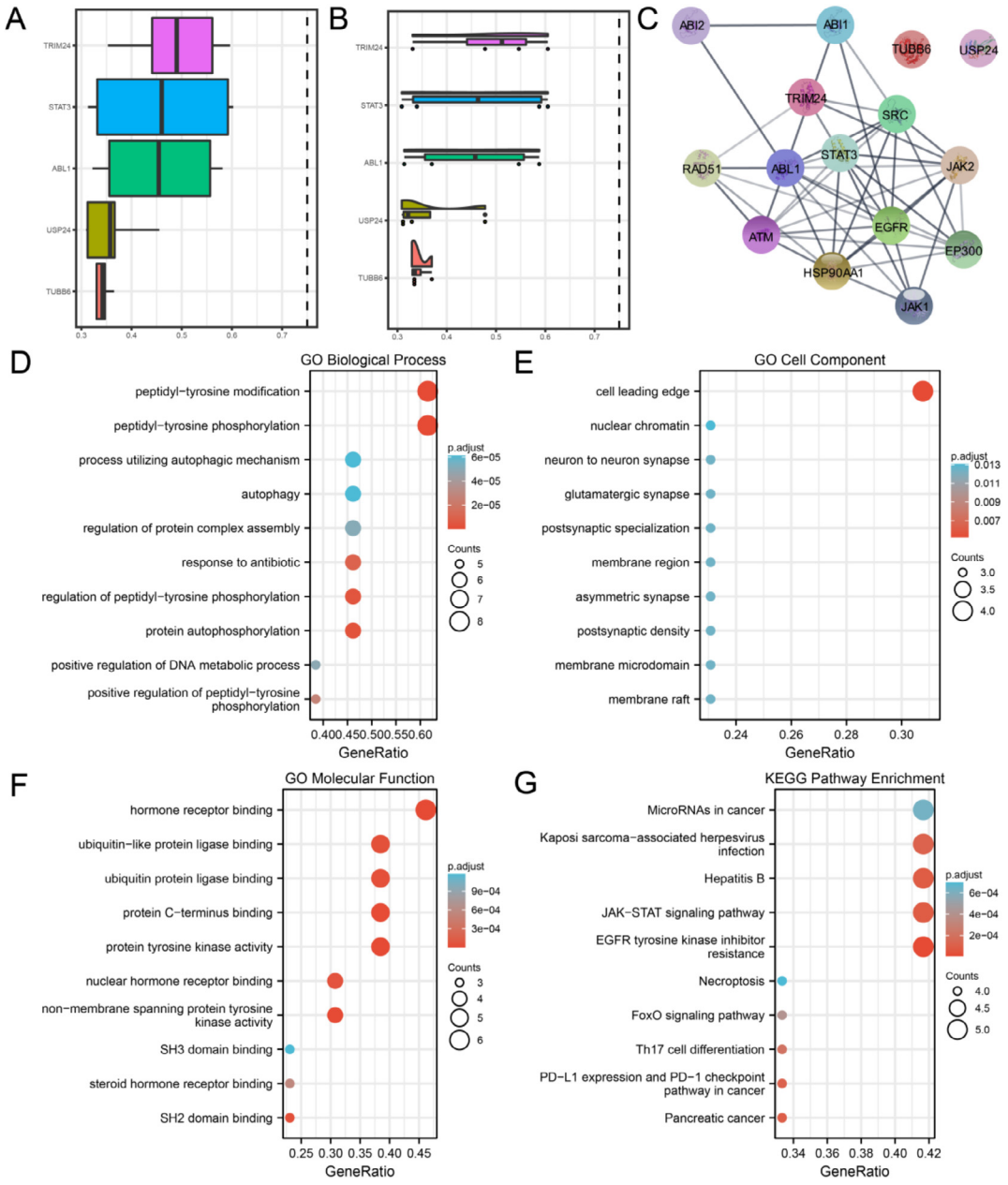

Fig. 3. Friends, GO, and KEGG enrichment analysis for pyroptosis-related DEGs. Friends analysis of DEPRGs. Bar diagrams (A), Functional similarity analysis diagram (B). The PPI network of DEPRGs (C). Bubble map of GO functional enrichment analysis results of DEPRGs: the GO BP category (D), the GO CC category (E), and the GO MF category (F). Bubble map of the KEGG enrichment analysis of DEPRGs (G). DEPRGs: differentially expressed pyroptosis-related genes, GO: Gene Ontology, MF: molecular function, BP: biological process, CC: cellular component, KEGG: Kyoto Encyclopedia of Genes and Genomes.

Table 2
Results of GO biology process analysis.

ID	Description	GeneRatio	BgRatio	*p* value	*p* adjust	*q* value
GO:0018108	Peptidyl-tyrosine phosphorylation	8/13	363/18670	2.24e-11	1.91e-08	6.76e-09
GO:0018212	Peptidyl-tyrosine modification	8/13	366/18670	2.39e-11	1.91e-08	6.76e-09
GO:0046777	Protein autophosphorylation	6/13	235/18670	5.95e-09	3.17e-06	1.12e-06
GO:0050730	Regulation of peptidyl-tyrosine phosphorylation	6/13	256/18670	9.92e-09	3.97e-06	1.41e-06
GO:0046677	Response to antibiotic	6/13	327/18670	4.27e-08	9.91e-06	3.51e-06
GO:0050731	Positive regulation of peptidyl-tyrosine phosphorylation	5/13	192/18670	1.31e-07	2.63e-05	9.30e-06
GO:0051054	Positive regulation of DNA metabolic process	5/13	228/18670	3.09e-07	4.94e-05	1.75e-05
GO:0043254	Regulation of protein complex assembly	6/13	467/18670	3.51e-07	5.10e-05	1.81e-05
GO:0006914	Autophagy	6/13	496/18670	5.00e-07	6.15e-05	2.18e-05
GO:0061919	Process utilizing autophagic mechanism	6/13	496/18670	5.00e-07	6.15e-05	2.18e-05

GO: Gene Ontology.

CC) highlighted membrane raft organization (Fig. 3E and Table 3), while molecular function (GO-MF) analysis identified enriched terms, including tyrosine kinase activity and SH2 domain binding (Fig. 3F and Table 4). KEGG pathway analysis indicated a strong enrichment of genes participating in the JAK–STAT signaling cascade, Th17 cell differentiation, EGFR-TKI resistance, and FoxO signaling, which links metabolic regulation with inflammation (Fig. 3G and Table 5). Collectively, these findings underscore the participation of DEPRGs in key inflammatory signaling cascades relevant to DR.

3.3. Hub gene identification

Using five cytoHubba algorithms (degree, MNC, MCC, closeness, and EPC), a consensus analysis identified nine hub genes: ABL1, EGFR, HSP90AA1, SRC, JAK2, STAT3, ATM, EP300, and JAK1 (Fig. 4A–F). These genes function as central nodes within the interaction network, suggesting their central involvement in coordinating signaling events that govern pyroptotic activity.

3.4. Immune microenvironment alterations

CIBERSORTx analysis of the GSE12610 dataset revealed significant alterations in immune cell composition in DR retinas (Fig. 5A). DR samples showed increased infiltration of T follicular helper (Tfh) cells and M0 macrophages, accompanied by a pronounced reduction in resting memory $CD4^+$ T cells, resting natural killer (NK) cells, and M2 macrophages relative to controls (Fig. 5B). Correlation analysis demonstrated that TUBB6 expression was inversely associated with the abundance of resting memory $CD4^+$ T cells ($p = 0.037$) and positively correlated with Tfh cell infiltration ($p = 3.97 \times 10^{-24}$), supporting a link between pyroptosis-related gene expression and immune dysregulation (Fig. 5C–G and Table 6).

3.5. Multi-layered regulatory network construction

PPI mapping revealed direct interactions among ABL1, STAT3, and TRIM24 (Fig. 6A). Analysis of the miRTarBase and StarBase

Table 3
GO cell component analysis.

ID	Description	GeneRatio	BgRatio	*p* value	*p* adjust	*q* value
GO:0031252	Cell leading edge	4/13	403/19717	1.06e-04	0.005	0.003
GO:0045121	Membrane raft	3/13	315/19717	0.001	0.012	0.006
GO:0098857	Membrane microdomain	3/13	316/19717	0.001	0.012	0.006
GO:0014069	Postsynaptic density	3/13	324/19717	0.001	0.012	0.006
GO:0032279	Asymmetric synapse	3/13	328/19717	0.001	0.012	0.006
GO:0098589	Membrane region	3/13	328/19717	0.001	0.012	0.006
GO:0099572	Postsynaptic specialization	3/13	348/19717	0.001	0.012	0.006
GO:0098978	Glutamatergic synapse	3/13	349/19717	0.001	0.012	0.006
GO:0098984	Neuron-to-neuron synapse	3/13	350/19717	0.001	0.012	0.006
GO:0000790	Nuclear chromatin	3/13	377/19717	0.002	0.013	0.006

GO: Gene Ontology.

Table 4
Results of GO molecular function analysis.

ID	Description	GeneRatio	BgRatio	*p* value	*p* adjust	*q* value
GO:0051427	Hormone receptor binding	6/13	185/17697	1.94e-09	2.60e-07	8.39e-08
GO:0004715	Nonmembrane-spanning protein tyrosine kinase activity	4/13	46/17697	2.81e-08	1.26e-06	4.07e-07
GO:0004713	Protein tyrosine kinase activity	5/13	134/17697	2.83e-08	1.26e-06	4.07e-07
GO:0008022	Protein C-terminus binding	5/13	187/17697	1.50e-07	5.03e-06	1.62e-06
GO:0031625	Ubiquitin protein ligase binding	5/13	290/17697	1.32e-06	3.54e-05	1.14e-05
GO:0044389	Ubiquitin-like protein ligase binding	5/13	308/17697	1.77e-06	3.96e-05	1.28e-05
GO:0042169	SH2 domain binding	3/13	36/17697	2.18e-06	4.17e-05	1.34e-05
GO:0035257	Nuclear hormone receptor binding	4/13	152/17697	3.52e-06	5.90e-05	1.90e-05
GO:0035258	Steroid hormone receptor binding	3/13	92/17697	3.74e-05	5.58e-04	1.80e-04
GO:0017124	SH3 domain binding	3/13	130/17697	1.05e-04	0.001	3.78e-04

GO: Gene Ontology.

Table 5
Results of KEGG analysis.

ID	Description	GeneRatio	BgRatio	*p* value	*p* adjust	*q* value
hsa01521	EGFR tyrosine kinase inhibitor resistance	5/12	79/8076	5.92e-08	6.51e-06	3.36e-06
hsa04630	JAK-STAT signaling pathway	5/12	162/8076	2.16e-06	7.91e-05	4.09e-05
hsa05161	Hepatitis B	5/12	162/8076	2.16e-06	7.91e-05	4.09e-05
hsa05212	Pancreatic cancer	4/12	76/8076	3.39e-06	9.31e-05	4.81e-05
hsa05167	Kaposi sarcoma-associated herpesvirus infection	5/12	193/8076	5.12e-06	1.13e-04	5.82e-05
hsa05235	PD-L1 expression and PD-1 checkpoint pathway in cancer	4/12	89/8076	6.38e-06	1.17e-04	6.04e-05
hsa04659	Th17 cell differentiation	4/12	107/8076	1.33e-05	2.09e-04	1.08e-04
hsa04068	FoxO signaling pathway	4/12	131/8076	2.96e-05	4.07e-04	2.10e-04
hsa05206	MicroRNAs in cancer	5/12	310/8076	5.12e-05	6.25e-04	3.23e-04
hsa04217	Necroptosis	4/12	159/8076	6.33e-05	6.97e-04	3.60e-04

KEGG: Kyoto Encyclopedia of Genes and Genomes.

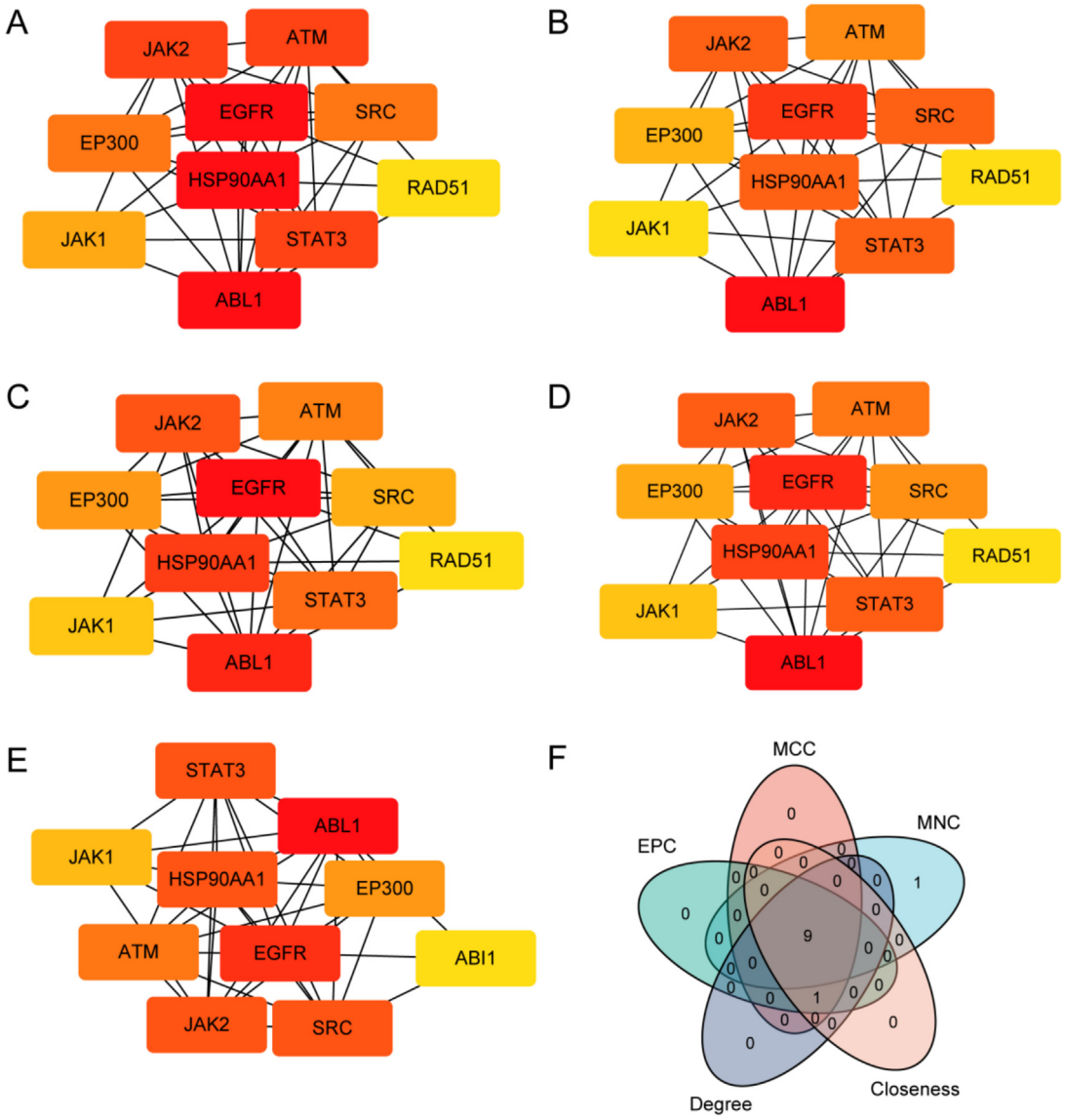

Fig. 4. Hub gene analysis by using the CytoHubba algorithm. Hub gene analysis by using the CytoHubba algorithm. MNC (A); degree (B); MCC (C); closeness (D); EPC (E). The block color from red to yellow represents the score from high to low. Venn diagrams for the top 10 genes from five algorithms (F). MNC, Maximum neighborhood component; MCC, Maximal clique centrality; EPC, Edge percolated component. (For interpretation of the references to color in this figure legend, the reader is referred to the web version of this article).

databases identified 15 microRNAs (miRNAs) that regulate four DEPRGs (USP24, ABL1, STAT3, and TUBB6), which were further linked to 57 lncRNAs and 32 circRNAs, forming a robust competing endogenous RNA (ceRNA) regulatory network (Fig. 6B, C). RBP analysis uncovered 98 interactions converging on nine RBPs, including IGF2BP1-3, eIF4AIII, FMRP, LIN28A/B, HuR, and PTB (Fig. 7A). In parallel, 63 TFs were identified as regulators of the five DEPRGs (Fig. 7B), and 75 potential therapeutic agents targeting these genes were retrieved (Fig. 7C). These results illustrate a comprehensive regulatory landscape spanning transcriptional, post-transcriptional, and pharmacological dimensions.

3.6. Validation and diagnostic efficacy of DEPRGs

The expression profiles of the five DEPRGs were validated in both datasets. In GSE12610, STAT3 and TUBB6 levels were significantly elevated in DR retinas (Fig. 8A). In GSE111465, USP24, STAT3, and ABL1 were upregulated, while TRIM24 and TUBB6 were significantly downregulated in DR samples compared to controls ($p < 0.05$; Fig. 8B). Diagnostic value was assessed through ROC analysis. Notably, in the GSE111465 dataset, the AUC values for TUBB6 and STAT3 exceeded 0.9, indicating high diagnostic accuracy (Fig. 8C, D).

3.7. High glucose induces pyroptosis and alters gene expression in MRMECs

To experimentally confirm pyroptosis under diabetic conditions, SEM was employed to examine MRMEC morphology following high-glucose exposure. Cells displayed hallmark pyroptotic features, including membrane pore formation and prominent cellular swelling (Fig. 9A-I). Biochemical assays revealed notably enhanced extracellular release of LDH, IL-1β, and IL-18, confirming pyroptotic cytolysis (Fig. 10A–C). Concurrently, qRT-PCR and

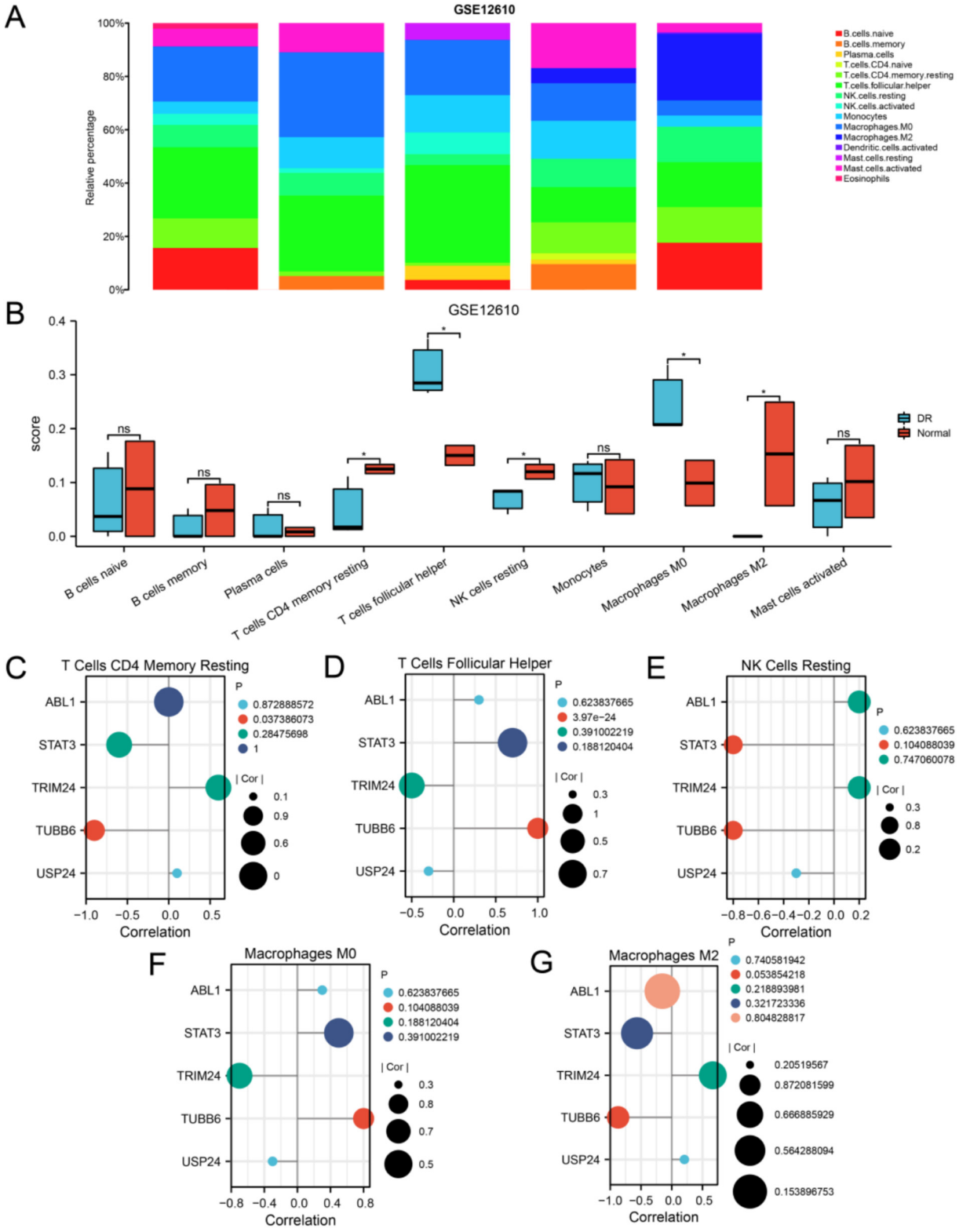

Fig. 5. Immune infiltration analysis by the CIBERSORTx algorithm. (A) The ratio of 22 immune cells in each DR mouse retina sample in GEO12610. (B) The proportions of immune cells in DR mouse retinas and control retinas. C-G The correlation between immune cells and DEPRGs: resting memory CD4 T cells (C), follicular helper T cells (D), resting NK cells (E), M0 macrophages (F), and M2 macrophages (G). DEPRGs: differentially expressed pyroptosis-related genes, DR: diabetic retinopathy.

Western blot analyses showed upregulation of STAT3, ABL1, and USP24 and downregulation of TRIM24, whereas TUBB6 showed no significant change in response to hyperglycemia (Fig. 10D–I). These findings suggest that dysregulation of these DEPRGs contributes directly to pyroptotic processes in the diabetic retinal microvasculature.

Table 6
GSE12610 CIBERSORTx.

	USP24 *p*	TUBB6 *p*	TRIM24 *p*	STAT3 *p*	ABL1 *p*	USP24 cor	TUBB6 cor	TRIM24 cor	STAT3 cor	ABL1 cor
B.cells. naive	0.805	0.935	0.172	0.614	0.741	0.154	−0.051	0.718	0.308	0.205
B.cells. memory	0.858	0.45	0.45	0.215	0.718	−0.112	−0.447	−0.447	−0.671	−0.224
Plasma. Cells	0.718	0.718	0.581	0.858	0.118	0.224	0.224	−0.335	−0.112	−0.783
T. Cell.CD4. memory. Resting	0.873	0.037	0.285	0.285	1	0.100	−0.900	0.600	−0.600	0.000
T. cells. follicular. helper	0.624	0	0.391	0.188	0.624	−0.300	1.000	−0.500	0.700	0.300
NK. cells. Resting	0.624	0.104	0.747	0.104	0.747	−0.300	−0.800	0.200	−0.800	0.200
Monocytes	0.747	1	0.391	0.624	0.188	0.200	0.000	−0.500	−0.300	−0.700
Macrophages.M0	0.624	0.104	0.188	0.391	0.624	−0.300	0.800	−0.700	0.500	0.300
Macrophages.M2	0.741	0.054	0.219	0.322	0.805	0.205	−0.872	0.667	−0.564	−0.154
Mast. cells. Activated	0.873	0.285	0.873	0.391	0.873	0.100	−0.600	−0.100	−0.500	−0.100

p: p value; cor: cor value.

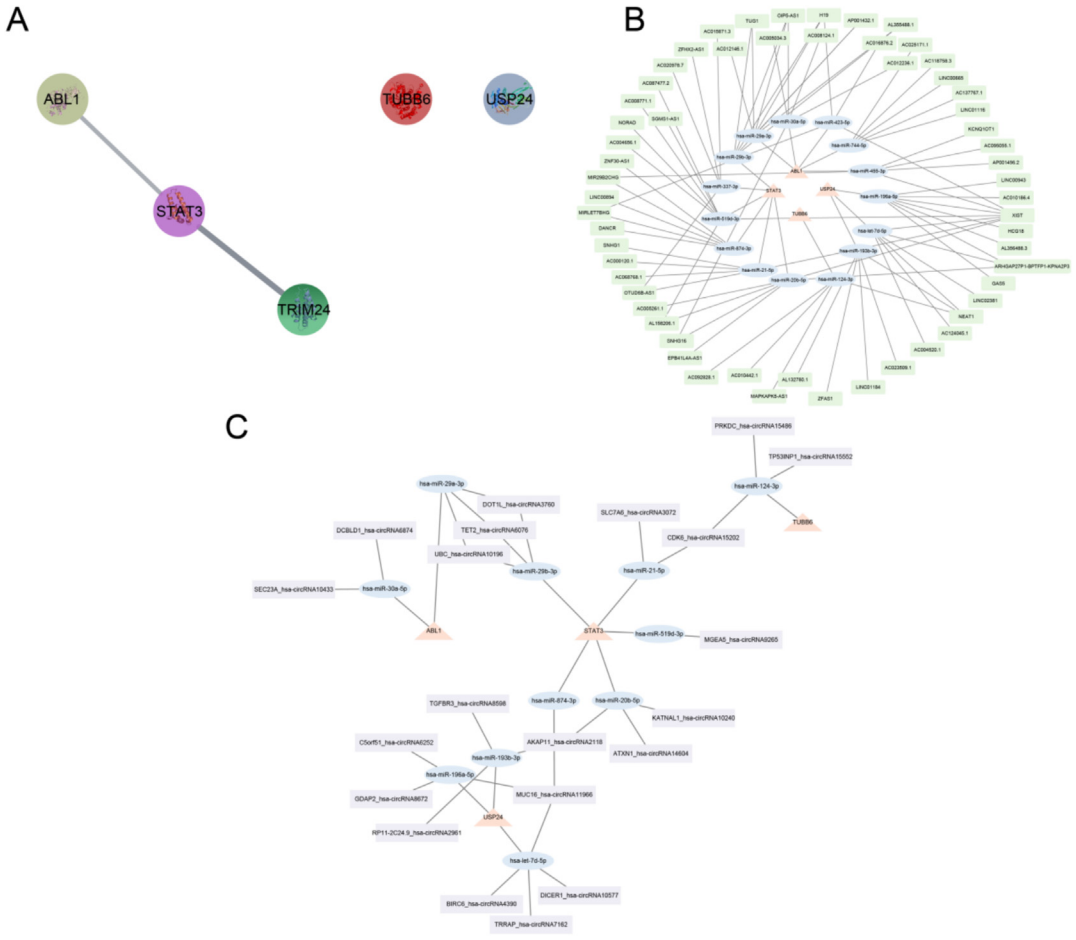

Fig. 6. Protein–protein interaction network and ceRNA regulation network. (A) PPI network of DEPRGs. (B) mRNA-miRNA-lncRNA regulatory network. (C) mRNA-miRNA-circRNA regulatory network. DEPRGs: differentially expressed pyroptosis-related genes; PPI, protein-protein interaction network.

3.8. The ABL1-STAT3 axis is essential for high glucose-induced pyroptosis in MRMECs

Given the central role of the NLRP3 inflammasome and its downstream effector GSDMD in pyroptosis, we focused on validating the predicted interaction between ABL1 and STAT3. Our earlier PPI network analyses highlighted this interaction as potentially critical in DR-related pyroptosis (Fig. 3C, Fig. 6A). Gene knockdown experiments in high glucose-treated MRMECs showed that silencing either ABL1 or STAT3 markedly suppressed the expression of pyroptotic markers, including IL-1β, IL-18, LDH, NLRP3, Cleaved Caspase-1, GSDMD-N, and ASC (Fig. 11A–D). To examine their hierarchical relationship, rescue experiments were performed by overexpressing ABL1 while simultaneously knocking down STAT3. This intervention reversed the pyroptotic effects of ABL1 overexpression, suggesting that STAT3 acts downstream of ABL1 in the

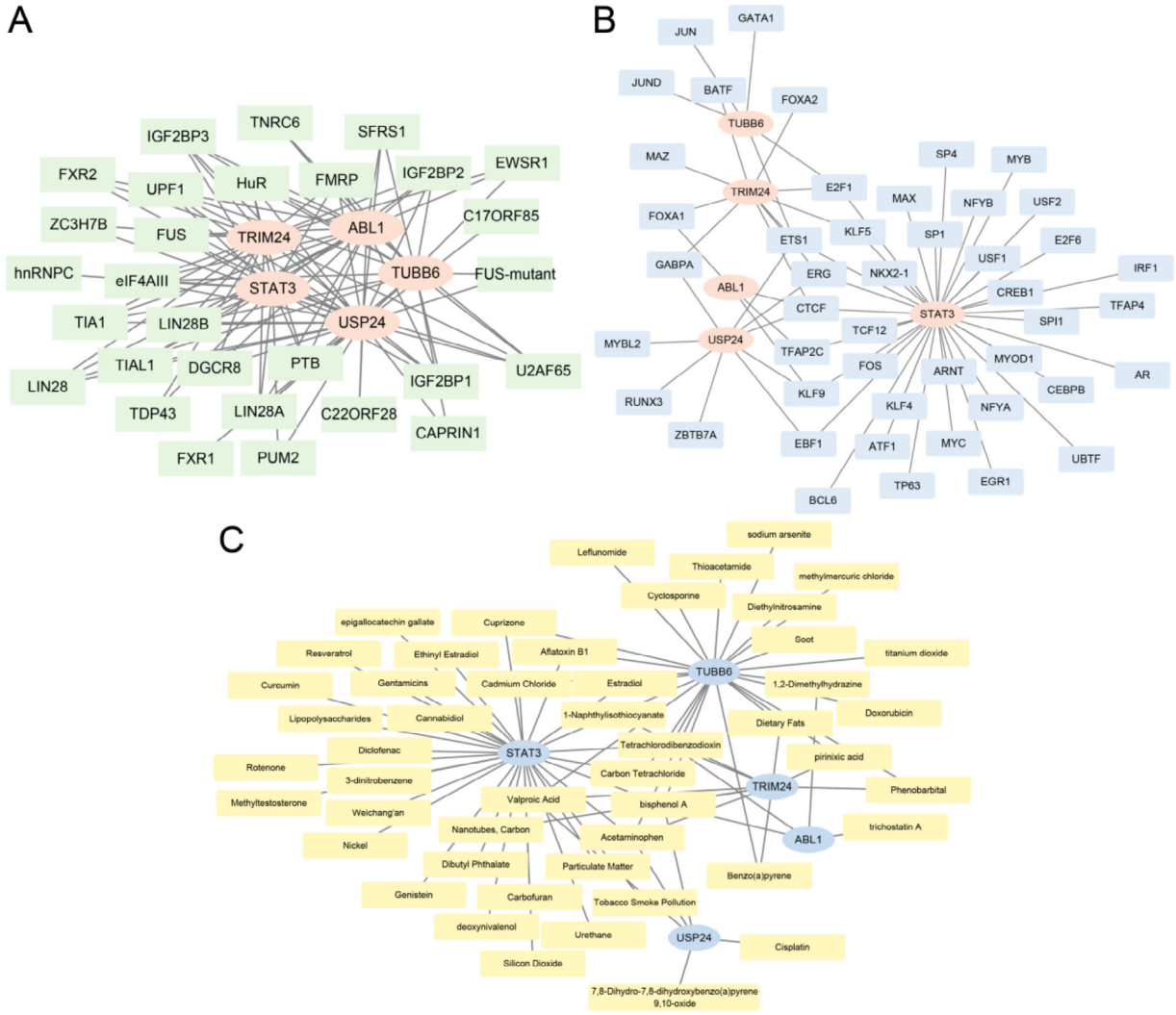

Fig. 7. Mrna-rbp, mrna-tf, and mrna-drug regulatory networks. (A) mRNA-RBP regulatory network. (B) mRNA-TF regulatory network. (C) mRNA-drug regulatory network. RBP, RNA-binding protein; TF, Transcription factor.

signaling cascade (Fig. 11E). These results identify an ABL1–STAT3 regulatory axis as a critical driver of high glucose-induced pyroptosis in DR pathogenesis.

4. Discussion

Despite the availability of clinical treatments, current therapeutic strategies for DR often fail to deliver sustained efficacy, partly due to systemic side effects and high rates of disease recurrence. This highlights the pressing need to unravel the precise molecular mechanisms that drive DR pathogenesis and progression [12]. Recent studies have identified pyroptosis, an inflammation-driven form of programmed cell death, as a central pathogenic process contributing to retinal damage under diabetic conditions [13]. While elevated levels of pyroptotic markers have been observed in DR, a systematic dissection of its regulatory network has been lacking. In this study, we identified five key DEPRGs, USP24, STAT3, and ABL1 (upregulated), along with TRIM24 and TUBB6 (downregulated), that are strongly associated with DR. Our data revealed a coherent molecular cascade centered on the ABL1–STAT3–NLRP3 axis, which functions as a core regulatory module in diabetic retinal pyroptosis. This finding significantly enhances our understanding of how inflammatory cell death is orchestrated under hyperglycemic stress. Pyroptosis is defined by cellular swelling, the formation of membrane pores, and the extracellular discharge of inflammatory mediators such as IL-1β, IL-18, and LDH. To replicate the diabetic microenvironment, we cultured MRMECs after 48 h of exposure to high-glucose conditions. Pyroptosis was confirmed through multiple approaches: scanning electron microscopy visualized classical morphological features, while biochemical assays detected elevated extracellular IL-1β, IL-18, and LDH. Notably, the concurrent dysregulation of the five candidate DEPRGs in this model supports their strong association with the pyroptotic phenotype in retinal endothelial cells. Among these genes, STAT3 functions as a central transcription factor activated by phosphorylation in response to diverse cytokines and growth factors, including IFN, EGF, IL-6, HGF, and BMP2. Once phosphorylated, STAT3 dimerizes and translocates to the nucleus, where it promotes target transcription [14]. STAT3 regulates pyroptosis by transcriptionally activating genes such as NLRP3, ASC, and members of the gasdermin family [15]. Elevated STAT3 or p-STAT3 levels have been detected in DR models and patient samples [16]. Moreover, studies have demonstrated that the circZNF532/miR-20b-5p/STAT3 regulatory axis can modulate pyroptosis in DR: circZNF532 is elevated in DR serum and retina, while miR-20b-5p is suppressed [17]. Luciferase reporter assays confirmed

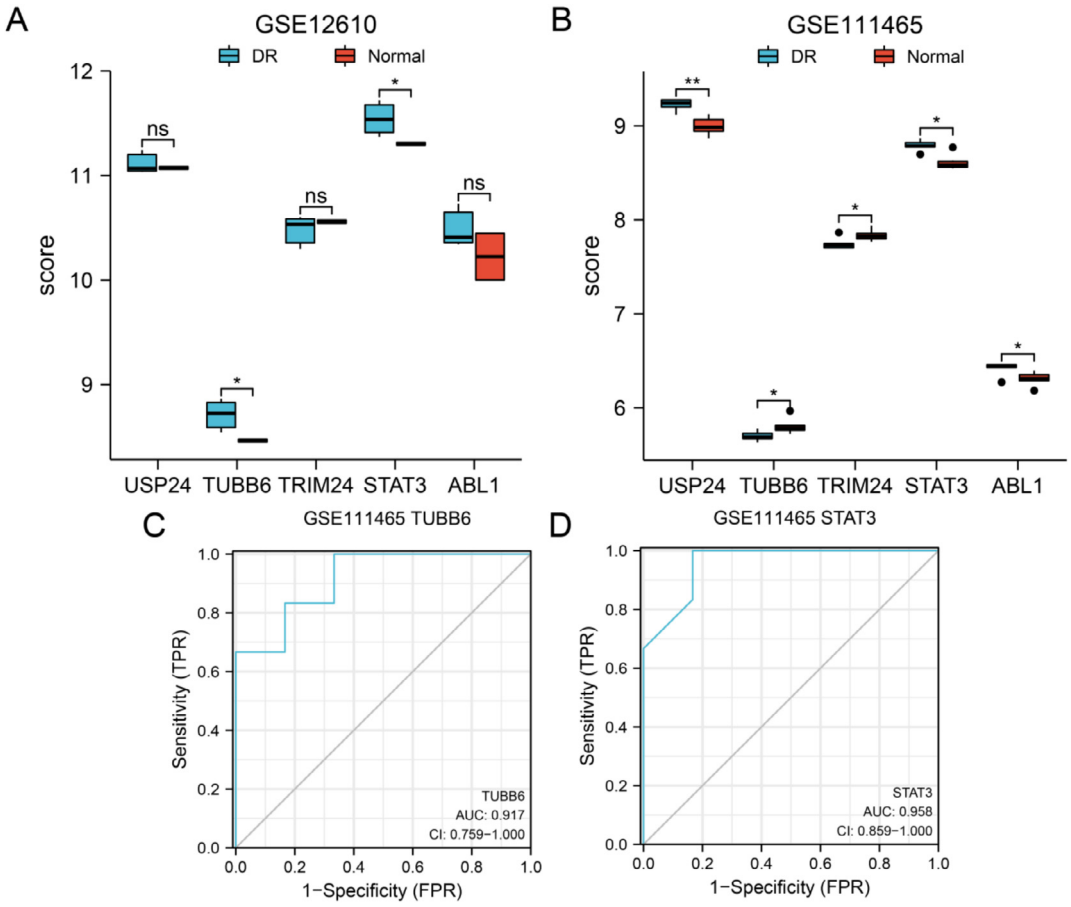

Fig. 8. Validation datasets and ROC curve analysis. Group comparison plots of analysis results of expression differences of DEPRGs in dataset GSE12610 (A) and dataset GSE111465 (B). ROC curves of the key genes TUBB6 (C) and STAT3 (D) in the GSE111465 dataset. *p value < 0.05; **p value < 0.01. DEPRGs: differentially expressed pyroptosis-related genes; ROC, receiver operating characteristic.

that miR-20b-5p directly targets STAT3. Knocking down circZNF532 leads to increased miR-20b-5p and decreased STAT3 expression, effectively inhibiting pyroptosis in retinal cells [18]. Tripartite Motif Containing 24 (TRIM24) is a nuclear transcriptional coactivator and E3 ubiquitin ligase. It modulates gene expression by interacting with nuclear receptors and influences protein degradation via its ligase activity [19]. TRIM24 regulates TP53 stability and suppresses NLRP3/CASP1/IL-1β-mediated pyroptosis by ubiquitinating NLRP3 in endometriosis [20]. TRIM24 also physically interacts with STAT3 to enhance its transcriptional activity [21]. USP24 encodes a deubiquitinating enzyme that modulates protein stability and cell survival by regulating substrates such as DDB2, MCL1, and TP53 [22]. Recent findings indicate that USP24 can stabilize GSDMB and activate the STAT3 pathway, thereby promoting pyroptosis in bladder cancer [23].

ABL1, a nonreceptor tyrosine kinase, promotes the activation of STAT3 through phosphorylation [24]. ABL1-mediated phosphorylation of RNF213 can enhance NF-κB signaling and, when combined with hypoxia-induced endoplasmic reticulum stress, promote GSDMD-dependent pyroptosis, as observed in diseases such as moyamoya and atherosclerosis [25]. Our study confirmed that ABL1 operates upstream of STAT3. Rescue experiments showed that STAT3 knockdown effectively reversed the pyroptotic effects induced by ABL1 overexpression, thereby validating the existence of a functionally important ABL1–STAT3 signaling axis in DR. TUBB6, a core component of the microtubule cytoskeleton, is known to disrupt microtubule networks when overexpressed, impairing cellular stability [26]. Previous studies suggest that TUBB6 knockdown or microtubule stabilization can inhibit pyroptosis independently of caspase-1 activation [27]. In our bioinformatic screening, TUBB6 was identified as a DEPRG, showing downregulation in the GSE111465 dataset with a high diagnostic AUC (>0.9). However, its expression trend was inconsistent across datasets (upregulated in GSE12610), and more importantly, in our high-glucose-treated MRMECs, TUBB6 mRNA and protein levels remained unchanged. This discrepancy suggests that TUBB6 may not be directly regulated by acute hyperglycemia in this *in vitro* model, and its role in DR-associated pyroptosis requires further validation in human tissues or more complex disease models.

Our findings extend previous work by identifying three novel circRNAs: hsa_circ_10240 (KATNAL1 host), hsa_circ_2118 (AKAP11 host), and hsa_circ_1460. These act as additional regulators of the miR-20b-5p/STAT3 axis and contribute to DR pathogenesis. We also highlight the strong diagnostic potential of STAT3, with AUC values exceeding 0.9 in the GSE111465 dataset, underscoring its translational value as a biomarker. Although TUBB6 also showed a high AUC in bioinformatic screening, its inconsistent expression profile necessitates further validation of its diagnostic utility. Functional enrichment analysis further reinforced these observations by identifying significant involvement of tyrosine kinase activity, SH2 domain binding, and JAK-STAT signaling. These pathways are tightly linked to inflammation and immune responses in DR. Moreover, our identification of RBPs with m6A-related functions points to an additional layer of posttranscriptional regulation. IGF2BP1–3 and FMRP function as m6A readers, stabilizing and enhancing the translation of their targets [28,29]. eIF4AIII, a core

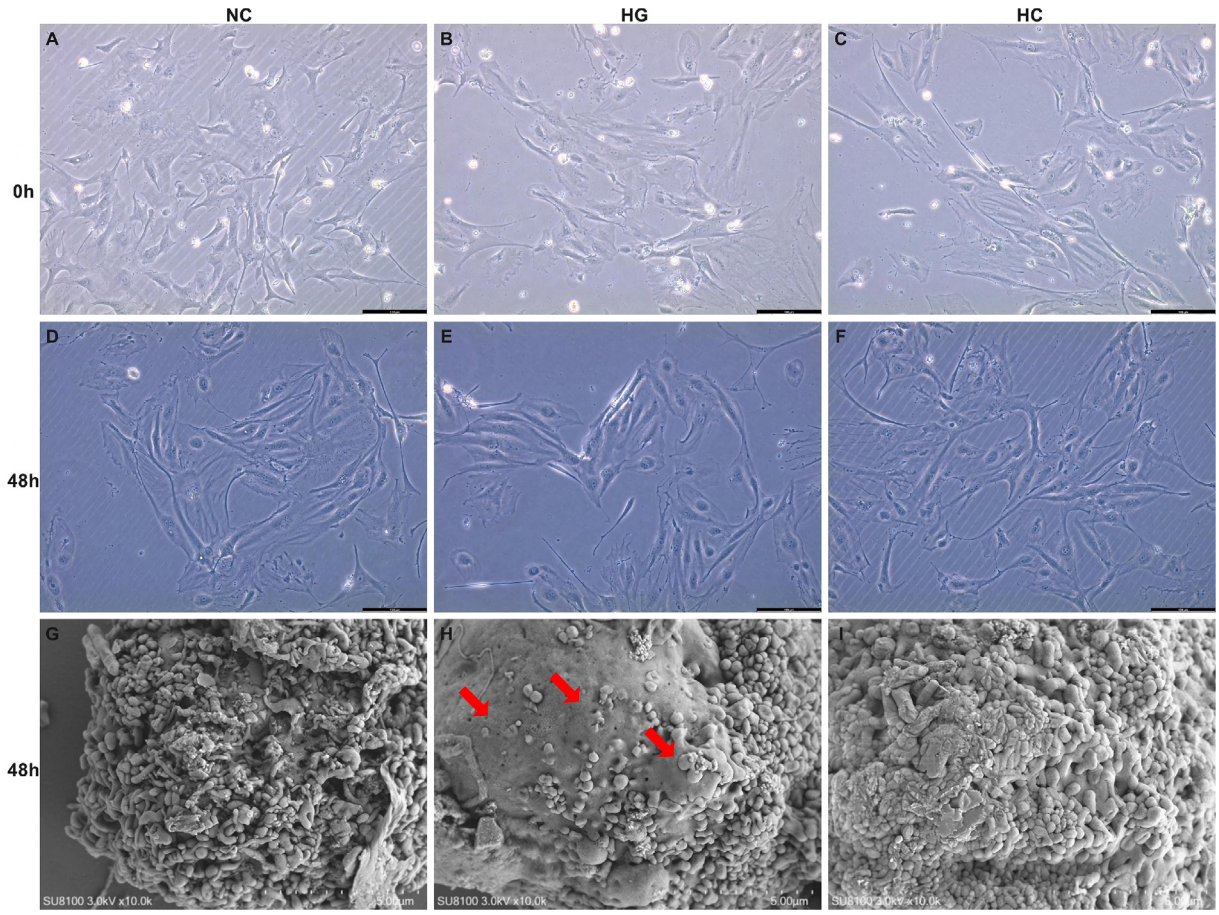

Fig. 9. High glucose induces pyroptosis in mouse retinal microvascular endothelial cells (MRMECs). (A–I) Scanning electron microscopy (SEM) images of MRMECs cultured under normal glucose (NG, 5 mM D-glucose), hypertonic control (HC, 5 mM D-glucose + 25 mM D-mannitol), or high glucose (HG, 30 mM D-glucose) conditions for 48 h. Red arrows indicate characteristic pyroptotic morphology, including plasma membrane bubbling and pore formation. Scale bar, 5 μm. (For interpretation of the references to color in this figure legend, the reader is referred to the web version of this article.)

component of the exon junction complex, also influences m6A-modified mRNA stability and localization [30]. HuR competes with YTHDF-mediated degradation to stabilize m6A-modified transcripts [31]. These interactions suggest that epitranscriptional modifications may fine-tune the expression of pyroptosis-related genes. Supporting this, Long Suo et al. [28] reported elevated m6A methylation levels in diabetic pericytes and DR mouse retinas.

Our immune infiltration analysis provided additional insights into the inflammatory microenvironment of DR. We observed increased proportions of Tfh cells and M0 macrophages in DR retinas, along with decreased levels of resting memory CD4+ T cells, NK cells, and M2 macrophages. These results align with prior studies demonstrating increased Tfh cell infiltration and reduced NK cell functionality in DR patients [32,33,34]. M2 macrophages have been observed in the vitreous and fibrovascular membranes of proliferative DR patients and in DR rat retinas [33,35,36]. Correlation analysis revealed that TUBB6 expression in the dataset showed a positive correlation with Tfh cell infiltration and a negative correlation with resting CD4+ memory T cells. These bioinformatic associations suggest that TUBB6 might be linked to immune cell reprogramming in the diabetic retina, although its direct functional role in our experimental model was not confirmed. Despite the strengths of our multidimensional analysis, some limitations should be acknowledged. First, the generalizability of our findings to human DR requires careful consideration due to inherent interspecies differences. Second, and relatedly, all our experimental validations were conducted in MRMECs. This model was chosen to maintain methodological and biological consistency with the mouse-derived transcriptomic datasets (GSE12610, GSE111465) that informed our study, thereby providing a direct proof-of-concept. However, MRMECs may not fully recapitulate the complexity of the human retinal microenvironment. Therefore, future validation in human retinal cells (e.g., endothelial cells or RPE cells such as ARPE-19) and clinical tissues is essential to confirm the translational relevance of the ABL1-STAT3-NLRP3 axis. Third, the inconsistent expression profile of TUBB6 across datasets and its lack of response to high glucose in our MRMEC model indicate that its potential role as a DR biomarker necessitates further investigation in human cohorts.

5. Conclusions

This study combined bioinformatics screening with experimental validation to elucidate the molecular mechanisms underlying pyroptosis in DR. We identified a set of pyroptosis-associated genes, and functional investigations established the ABL1–STAT3–NLRP3 signaling axis as a novel, central driver of disease progression. Specifically, we demonstrate that hyperglycemia activates this axis to mediate NLRP3 inflammasome-dependent pyroptosis in retinal endothelial cells. Moreover, STAT3 exhibited strong diagnostic potential (AUC > 0.9), underscoring its translational value as a biomarker. Collectively, these findings reveal a key pathogenic circuit in DR and suggest that the ABL1-STAT3 interaction is a promising therapeutic target for attenuating

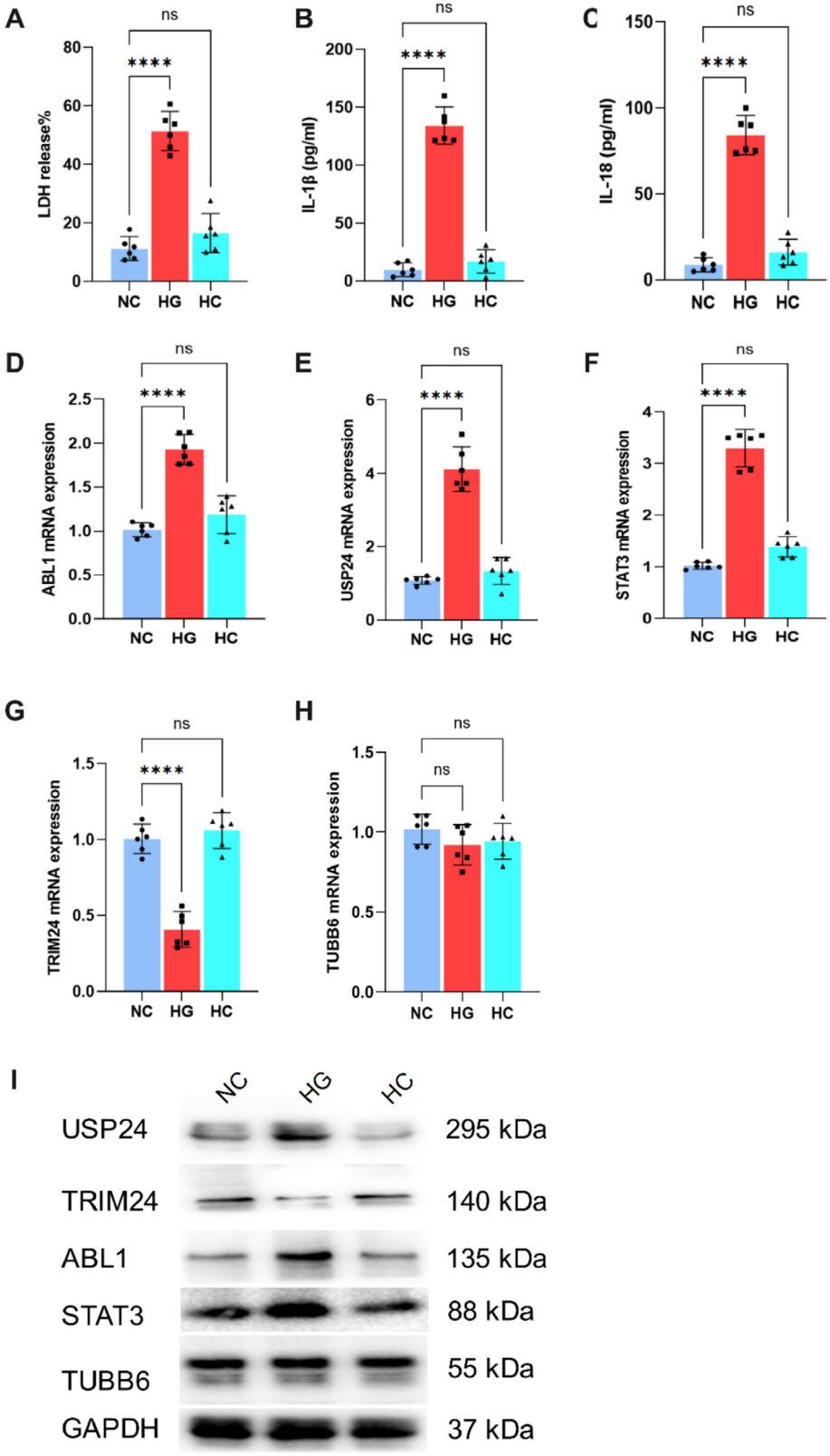

Fig. 10. HG induces dysregulation of pyroptosis-related gene expression in mouse retinal microvascular endothelial cells (MRMECs). (A-C) HG induces pyroptosis. (A) LDH release. (B) Mature IL-1β levels measured by ELISA. (C) Mature IL-18 levels measured by ELISA. (D-H) qRT-PCR validation of DEPRGs expression for ABL1 (D), USP24 (E), STAT3 (F), TRIM24 (G), and TUBB6 (H). (I) Western blot analysis. mRNA and Protein levels were normalized to GAPDH. Data are presented as mean ± SD (n = 3). Data were analyzed by one-way ANOVA followed by Dunnett's post hoc test. $^{****}p < 0.0001$ vs. the NG group; ns, not significant. Abbreviations: HG, high glucose; NC, normal control; HC, hypertonic control; DEPRGs: differentially expressed pyroptosis-related genes; MRMECs, mouse retinal microvascular endothelial cells; LDH, lactate dehydrogenase.

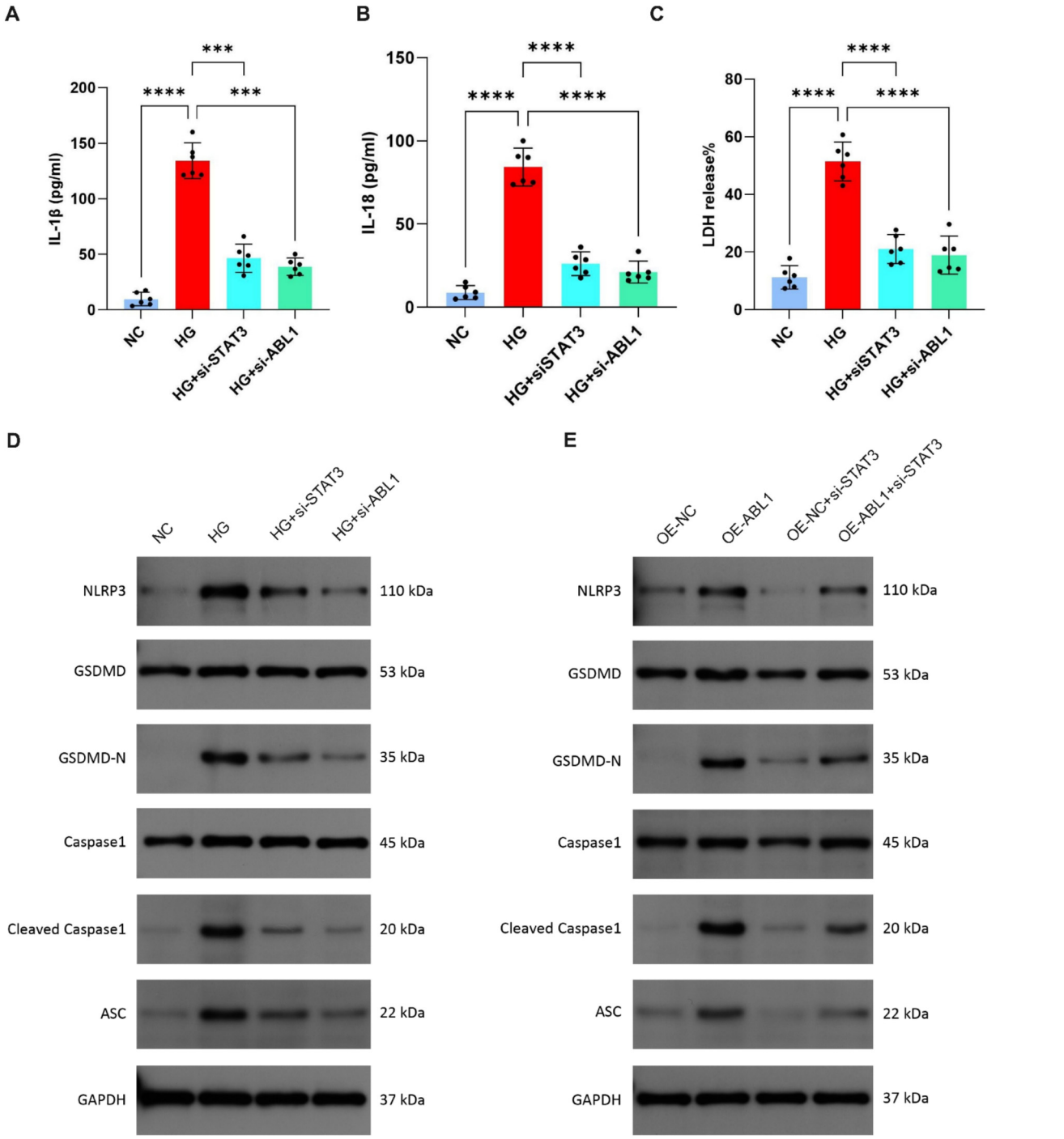

Fig. 11. The ABL1-STAT3 axis is essential for HG-induced pyroptosis in MRMECs. (A-D) Knockdown of STAT3 or ABL1 attenuates pyroptosis. (A) LDH release. (B) Mature IL-1β levels measured by ELISA. (C) Mature IL-18 levels measured by ELISA. (D) Western blot analysis. (E) STAT3 functions downstream of ABL1 in the pyroptotic pathway. Protein levels were normalized to GAPDH. Data are presented as mean ± SD (n = 3). Data were analyzed by one-way ANOVA followed by Dunnett's post hoc test. ***$p < 0.001$, ****$p < 0.0001$ vs. HG group; ns, not significant. Abbreviations: HG, high glucose; NC, normal control; HC, hypertonic control; MRMECs, mouse retinal microvascular endothelial cells; LDH, lactate dehydrogenase.

inflammation-induced retinal injury. Validation in human systems remains essential to advance these insights toward clinical application.

CRediT authorship contribution statement

Lili Hu: Writing – review & editing, Writing – original draft, Visualization, Validation, Software, Resources, Project administration, Methodology, Investigation, Funding acquisition, Formal analysis, Data curation, Conceptualization. **Gong Chen:** Visualization, Software, Methodology, Data curation. **Haoning Pan:** Validation. **Shaoxin Pan:** Writing – review & editing, Supervision, Funding acquisition.

Financial support

The Wuhu Science and Technology Bureau Project (2025kj057). The Natural Science Research Project of the Anhui Provincial

Department of Education (Major Project 2025AHGXZK20106 and Key Project 2025AHGXZK31442). The Clinical Medical Research Transformation Project of Anhui Province (202527c10020042). The Scientific Research Startup Fund Project for High-level Talents of the Second Affiliated Hospital of Wannan Medical College (GRK202507, GRK202518).

Declaration of competing interest

The authors declare that they have no competing interests.

Acknowledgments

We would like to thank all the participants in this study.

Supplementary data

https://doi.org/10.1016/j.ejbt.2026.100717.

Data availability

Data are available on https://www.jianguoyun.com/p/DVLEh9kQgNGbDhiM3Z4GIAA. The datasets used in this study were downloaded from GEO (https://www.ncbi.nlm.nih.gov/geo/). The PRGs were obtained from the GeneCards (https://www.genecards.org/), GSEA databases (https://www.gsea-msigdb.org/gsea/index.jsp), and PubMed. The R package used was obtained from Bioconductor (https://www.bioconductor.org/). All data generated or analyzed during this study are included in this published article. If readers have any questions about the data processing, please do not hesitate to contact us.

References

[1] Teo ZL, Tham YC, Yu M, et al. Global prevalence of diabetic retinopathy and projection of burden through 2045: Systematic review and meta-analysis. Ophthalmology 2021;128(11):1580–91. https://doi.org/10.1016/j.ophtha.2021.04.027. PMid: 33940045.

[2] Sivaprasad S, Wong TY, Gardner TW, et al. Diabetic retinal disease. Nat Rev Dis Primers 2025;11(1):62. https://doi.org/10.1038/s41572-025-00646-x. PMid: 40877334.

[3] Schmidt AM. Highlighting diabetes mellitus: The epidemic continues. Arteriosclerer Thromb Vasc Biol 2018;38(1):e1–8. https://doi.org/10.1161/ATVBAHA.117.310221. PMid: 29282247.

[4] Tan Y, Fukutomi A, Sun MT, et al. Anti-VEGF crunch syndrome in proliferative diabetic retinopathy: A review. Surv Ophthalmol 2021;66(6):926–32. https://doi.org/10.1016/j.survophthal.2021.03.001. PMid: 33705807.

[5] Hu L, Yang H, Ai M, et al. Inhibition of TLR4 alleviates the inflammation and apoptosis of retinal ganglion cells in high glucose. Graefe's Arch Clin Exp Ophthalmol 2017;255(11):2199–210. https://doi.org/10.1007/s00417-017-3772-0. PMid: 28808786.

[6] Meng C, Gu C, He S, et al. Pyroptosis in the retinal neurovascular unit: New insights into diabetic retinopathy. Front Immunol 2021;12:763092. https://doi.org/10.3389/fimmu.2021.763092. PMid: 34737754.

[7] Wang Y, Kanneganti TD. From pyroptosis, apoptosis and necroptosis to PANoptosis: A mechanistic compendium of programmed cell death pathways. Comput Struct Biotechnol J 2021;19:4641–57. https://doi.org/10.1016/j.csbj.2021.07.038. PMid: 34504660.

[8] Liu Y, Pan R, Ouyang Y, et al. Pyroptosis in health and disease: Mechanisms, regulation and clinical perspective. Signal Transduct Target Ther 2024;9(1):245. https://doi.org/10.1038/s41392-024-01958-2. PMid: 39300122.

[9] Zhang Y, Jiao Y, Li X, et al. Pyroptosis: A new insight into eye disease therapy. Front Pharmacol 2021;12:797110. https://doi.org/10.3389/fphar.2021.797110. PMid: 34925047.

[10] Chen M, Rong R, Xia X. Spotlight on pyroptosis: Role in pathogenesis and therapeutic potential of ocular diseases. J Neuroinflammation 2022;19(1):183. https://doi.org/10.1186/s12974-022-02547-2. PMid: 35836195.

[11] Al Mamun A, Mimi AA, Zaeem M, et al. Role of pyroptosis in diabetic retinopathy and its therapeutic implications. Eur J Pharmacol 2021;904:174166. https://doi.org/10.1016/j.ejphar.2021.174166. PMid: 33979651.

[12] Roy S, Kern TS, Song B, et al. Mechanistic insights into pathological changes in the diabetic retina: Implications for targeting diabetic retinopathy. Am J Pathol 2017;187(1):9–19. https://doi.org/10.1016/j.ajpath.2016.08.022. PMid: 27846381.

[13] Gu J, Geng K, Guo M, et al. Targeting pyroptosis: New insights into the treatment of diabetic microvascular complications. Evid Based Complement Alternat Med 2022;2022:5277673. https://doi.org/10.1155/2022/5277673. PMid: 36204129.

[14] Samad MA, Ahmad I, Hasan A, et al. STAT3 signaling pathway in health and disease. MedComm 2025;6(4):e70152. https://doi.org/10.1002/mco2.70152. PMid: 40166646.

[15] Chen B, Dong X, Zhang JL, et al. Natural compounds target programmed cell death (PCD) signaling mechanism to treat ulcerative colitis: A review. Front Pharmacol 2024;15:1333657. https://doi.org/10.3389/fphar.2024.1333657. PMid: 38405669.

[16] Hong L, Lin Y, Yang X, et al. A narrative review of STAT proteins in diabetic retinopathy: From mechanisms to therapeutic prospects. Ophthalmology and Theraphy 2022;11(6):2005–26. https://doi.org/10.1007/s40123-022-00581-0. PMid: 36208390.

[17] Liang GH, Luo YN, Wei RZ, et al. CircZNF532 knockdown protects retinal pigment epithelial cells against high glucose-induced apoptosis and pyroptosis by regulating the miR-20b-5p/STAT3 axis. J Diabetes Investig 2022;13(5):781–95. https://doi.org/10.1111/jdi.13722. PMid: 34839589.

[18] Wang N, Ding L, Liu D, et al. Molecular investigation of candidate genes for pyroptosis-induced inflammation in diabetic retinopathy. Front Endocrinol 2022;13:918605. https://doi.org/10.3389/fendo.2022.918605. PMid: 35957838.

[19] Yang SK, Han DH. The role of TRIM24 in allergic rhinitis. Allergy Asthma Immunol Res 2023;15(5):543–4. https://doi.org/10.4168/aair.2023.15.5.543. PMid: 37827975.

[20] Hang Y, Tan L, Chen Q, et al. E3 ubiquitin ligase TRIM24 deficiency promotes NLRP3/caspase-1/IL-1β-mediated pyroptosis in endometriosis. Cell Biol Int 2021;45(7):1561–70. https://doi.org/10.1002/cbin.11592. PMid: 33724611.

[21] Lv D, Li Y, Zhang W, et al. TRIM24 is an oncogenic transcriptional co-activator of STAT3 in glioblastoma. Nat Commun 2017;8(1):1454. https://doi.org/10.1038/s41467-017-01731-w. PMid: 29129908.

[22] Wang SA, Young MJ, Wang YC, et al. USP24 promotes drug resistance during cancer therapy. Cell Death Differ 2021;28(9):2690–707. https://doi.org/10.1038/s41418-021-00778-z. PMid: 33846536.

[23] He H, Yi L, Zhang B, et al. USP24-GSDMB complex promotes bladder cancer proliferation via activation of the STAT3 pathway. Int J Biol Sci 2021;17(10):2417–29. https://doi.org/10.7150/ijbs.54442. PMid: 34326684.

[24] Maycotte P, Gearheart CM, Barnard R, et al. STAT3-mediated autophagy dependence identifies subtypes of breast cancer where autophagy inhibition can be efficacious. Cancer Res 2014;74(9):2579–90. https://doi.org/10.1158/0008-5472.CAN-13-3470. PMid: 24590058.

[25] Bhardwaj A, Panepinto MC, Ueberheide B, et al. A mechanism for hypoxia-induced inflammatory cell death in cancer. Nature 2025;637(8045):470–7. https://doi.org/10.1038/s41586-024-08136-y. PMid: 39506105.

[26] Salinas RE, Ogohara C, Thomas MI, et al. A cellular genome-wide association study reveals human variation in microtubule stability and a role in inflammatory cell death. Mol Biol Cell 2014;25(1):76–86. https://doi.org/10.1091/mbc.e13-06-0294. PMid: 24173717.

[27] Randazzo D, Khalique U, Belanto JJ, et al. Persistent upregulation of the β-tubulin tubb6, linked to muscle regeneration, is a source of microtubule disorganization in dystrophic muscle. Hum Mol Genet 2019;28(7):1117–35. https://doi.org/10.1093/hmg/ddy418. PMid: 30535187.

[28] Suo L, Liu C, Zhang QY, et al. METTL3-mediated N^6-methyladenosine modification governs pericyte dysfunction during diabetes-induced retinal vascular complication. Theranostics 2022;12(1):277–89. https://doi.org/10.7150/thno.63441. PMid: 34987645.

[29] Zou Z, Wei J, Chen Y, et al. FMRP phosphorylation modulates neuronal translation through YTHDF1. Mol Cell 2023;83(23):4304–4317.e8. https://doi.org/10.1016/j.molcel.2023.10.028. PMid: 37949069.

[30] Hu Z, Chen G, Zhao Y, et al. Exosome-derived circCCAR1 promotes CD8 + T-cell dysfunction and anti-PD1 resistance in hepatocellular carcinoma. Mol Cancer 2023;22(1):55. https://doi.org/10.1186/s12943-023-01759-1. PMid: 36932387.

[31] Chen Y, Peng C, Chen J, et al. WTAP facilitates progression of hepatocellular carcinoma via m6A-HuR-dependent epigenetic silencing of ETS1. Mol Cancer 2019;18(1):127. https://doi.org/10.1186/s12943-019-1053-8. PMid: 31438961.

[32] Liu Y, Yang Z, Lai P, et al. Bcl-6-directed follicular helper T cells promote vascular inflammatory injury in diabetic retinopathy. Theranostics 2020;10(9):4250–64. https://doi.org/10.7150/thno.43731. PMid: 32226551.

[33] Meng Z, Chen Y, Wu W, et al. Exploring the immune infiltration landscape and M2 macrophage-related biomarkers of proliferative diabetic retinopathy. Front Endocrinol 2022;13:841813. https://doi.org/10.3389/fendo.2022.841813. PMid: 35692390.

[34] Yu H, Liu B, Wu G, et al. Dysregulation of circulating follicular helper T cells in type 2 diabetic patients with diabetic retinopathy. Immunol Res 2021;69(2):153–61. https://doi.org/10.1007/s12026-021-09182-8. PMid: 33625683.

[35] Yoshida S, Kobayashi Y, Nakama T, et al. Increased expression of M-CSF and IL-13 in vitreous of patients with proliferative diabetic retinopathy: Implications for M2 macrophage-involving fibrovascular membrane formation. Br J Ophthalmol 2015;99(5):629–34. https://doi.org/10.1136/bjophthalmol-2014-305860. PMid: 25355804.

[36] Wang JH, Kumar S, Liu GS. Bulk gene expression deconvolution reveals infiltration of M2 macrophages in retinal neovascularization. Invest Ophthalmol Vis Sci 2021;62(14):22. https://doi.org/10.1167/iovs.62.14.22. PMid: 34797904.